Impact of open-core threading dislocations on the performance of AlGaN metal-semiconductor-metal photodetectors

S. Walde,[a] M. Brendel, U. Zeimer, F. Brunner, S. Hagedorn, and M. Weyers

Ferdinand-Braun-Institut, Leibniz-Institut für Höchstfrequenztechnik (FBH), Gustav-Kirchhoff-Str. 4, 12489 Berlin, Germany

The influence of open-core threading dislocations on the bias-dependent external quantum efficiency (EQE) of bottom-illuminated $Al_{0.5}Ga_{0.5}N$/AlN metal-semiconductor-metal (MSM) photodetectors (PDs) is presented. These defects originate at the $Al_{0.5}Ga_{0.5}N$/AlN interface and terminate on the $Al_{0.5}Ga_{0.5}N$ surface as hexagonal prisms. They work as electrically active paths bypassing the $Al_{0.5}Ga_{0.5}N$ absorber layer and therefore alter the behavior of the MSM PDs under bias voltage. This effect is included in the model of carrier collection in the MSM PDs showing a good agreement with the experimental data. While such dislocations usually limit the device performance, the MSM PDs benefit by high EQE at a reduced bias voltage while maintaining a low dark current. *Published by AIP Publishing.* https://doi.org/10.1063/1.5010859

I. INTRODUCTION

Ultra-violet (UV) photodetectors (PDs) offer great potential for applications in various fields like science, military, medicine, and industries.[1–3] Using $Al_xGa_{1-x}N$ as the absorber material with bandgap energies between 3.4 eV for GaN and 6.2 eV for AlN,[4] gives the opportunity to adjust the detector's cut-off wavelength λ_{c-o} from 365 nm to 200 nm by altering the Al content x. With x > 0.4 and therefore λ_{c-o} < 280 nm, a solar blind UV PD is obtained, which is desirable for specific applications like the detection of corona discharges.[5] Advantages of the metal-semiconductor-metal (MSM) type PDs are that no intentional doping of the layers or ohmic contacts are needed, both of which are challenging to achieve for $Al_xGa_{1-x}N$ with a high Al-content. Combined with the planar electrode layout, an MSM PD is easy to fabricate. The main drawbacks are the limitation of the external quantum efficiency (EQE) by electrode shading and non-radiative recombination losses in the field-free regions of the device[6] and the need for a rather high external bias to obtain a sufficiently high EQE comparable to that of, e.g., p-i-n devices, which have been reported with a very high EQE of 0.89 at 0 V.[7] In order to address the shading issue, illumination from the substrate side (bottom illumination) has been investigated in the past for MSM PDs based on GaN[8] and AlGaN.[9,10] Recently, it was shown that bottom-illuminated $Al_{0.5}Ga_{0.5}N$/AlN MSM PD shows a bias dependent saturation of the EQE at high values of up to 0.7 above a specific voltage U_{sat}. In this paper, a reduction of the saturation voltage caused by open-core threading dislocations in the absorber layer is discussed.

II. EXPERIMENTAL

A. Epitaxy and processing of MSM PDs

The layer structure for the MSM PDs is shown in Fig. 1(a). All layers were grown by metal-organic vapor phase epitaxy (MOVPE) on 2-in. double-side polished c-plane sapphire substrates to enable high optical incoupling efficiency from the bottom side. First, a 500 nm AlN buffer layer with Al-polarity is grown on the sapphire followed by an unintentionally doped $Al_{0.5}Ga_{0.5}N$ absorber layer with thicknesses between 300 nm and 1400 nm for different samples. On the $Al_{0.5}Ga_{0.5}N$ surface, Pt/Ti/Au Schottky contacts are processed by the e-beam evaporation and lift-off technique. The electrodes with 395 μm length, 2 μm width, and 0.5 μm thickness at a spacing of 5 μm are aligned in an interdigitated pattern [Fig. 1(b)], which consists of 29 anode-cathode pairs forming an active device area of 400 μm × 400 μm.

B. Characterization

Photocurrent spectroscopy (PCS) measurements of single MSM PDs have been carried out on the wafer level. Via PCS, the EQE of an MSM PD is determined in dependence of the wavelength of the incoming light and the applied bias voltage. A 300 W Xe-lamp is used as the light source, which is filtered by a monochromator and split up by a Y-type UV-fiber. Thus, one part of the beam is focused on the MSM PD from the bottom side (in the active detector region only), while the other one is focused on a calibrated GaP photodiode. This gives the possibility of monitoring the incident optical power P_{opt} reaching the MSM PD. Currents are measured in the dark and under illumination using a Keithley 6487 pico-amperemeter to determine the generated photocurrent I_{photo} and calculate the EQE using the relation

$$EQE = \frac{I_{photo}}{P_{opt}} \cdot \frac{E_{opt}}{e},$$

with E_{opt} being the energy of the photons and e the elementary charge.

An optical microscope with Nomarski contrast and an atomic force microscope (AFM) are used to investigate the surface morphology. Focused ion beam (FIB) preparation
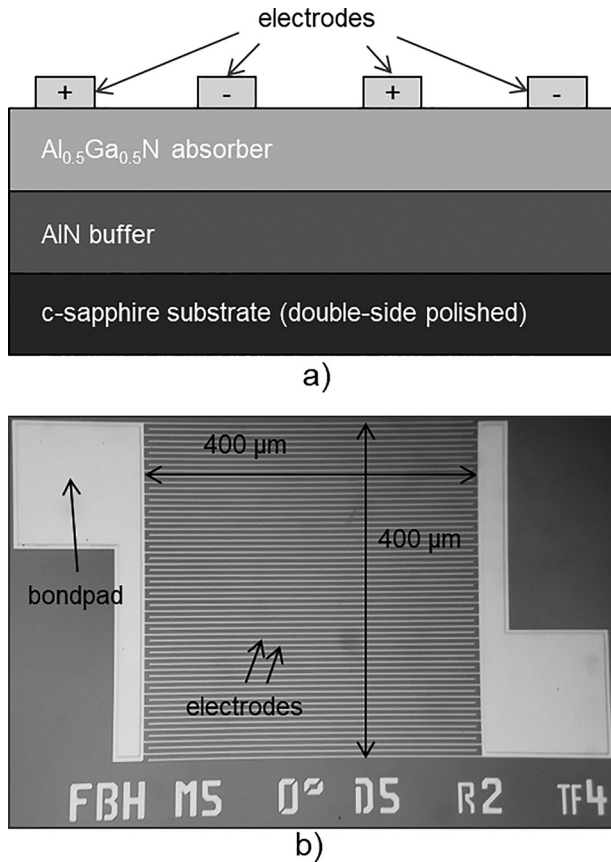
[a] Electronic mail: sebastian.walde@fbh-berlin.de

FIG. 1. Design of the solar-blind AlGaN MSM PDs: (a) cross-sectional sketch of the layer structure with the substrate at the bottom and the electrodes on the top. (b) Light microscopic plan-view image of the processed MSM PD on the wafer showing the interdigitated layout (dark: semiconductor, bright: metal).
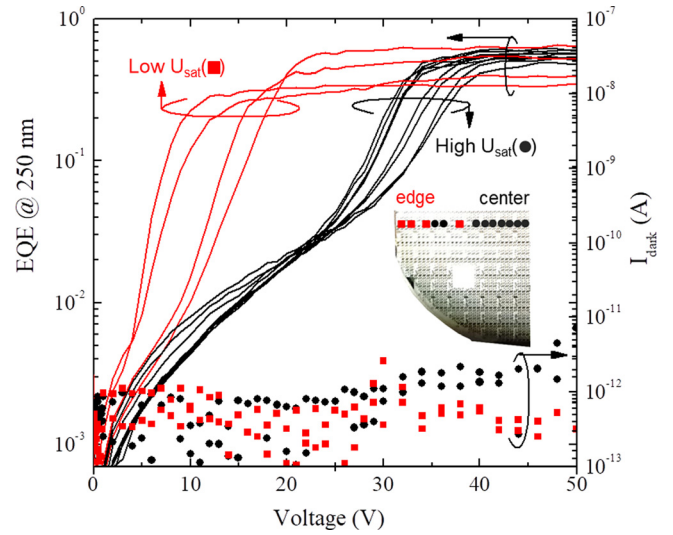

FIG. 2. EQE vs. bias characteristics of several MSM PDs illuminated from the bottom side at a wavelength of 250 nm along a 2-in. wafer from the center (black circles) to the edge (red squares). All devices show increasing EQE until saturation above U_{sat}, while values of U_{sat} vary between 10 V and 40 V. The dark currents I_{dark} for all devices are low (exemplarily shown for one MSM PD with high and one with low U_{sat}).

has been used for cross-section scanning electron microscopy (SEM) imaging.

III. RESULTS AND DISCUSSION

In Fig. 2, the measured EQE vs. bias characteristics of several bottom-illuminated MSM PDs on the same wafer with an absorber layer thickness of 500 nm are shown. For all detectors, saturation of the EQE at high values > 0.3 above a certain saturation voltage U_{sat} can be observed. For most of the detectors, the EQE in saturation is between 0.45 and 0.65. Only the two devices close to the wafer edge show somewhat lower values of around 0.35. This behaviour is generally observed and most probably due to inhomogenous layer properties. However, for some MSM PDs, U_{sat} is reduced by about 15–20 V in comparison to the majority of the devices. The lower U_{sat} is more frequent for devices located at the edge of the wafer while near the center most devices feature the high U_{sat} (insert in Fig. 2). The dark current I_{dark} for detectors with low or high U_{sat} does not differ significantly and remains near the measurement limit (pA) for voltages up to 50 V. The origin of saturation at high voltages (i.e., 20–30 V) in bottom-illuminated MSM PDs of the same epitaxial structure was analyzed by Brendel *et al.*[6] by means of two-dimensional drift diffusion modeling. Accordingly, the high EQE in saturation is achieved due to

the sweep-out of photogenerated holes accumulated in the polarization-induced space charge region (SCR) at the $Al_{0.5}Ga_{0.5}N/AlN$ interface, when the bias-dependent SCR below the rectifying Schottky contact reaches through the $Al_{0.5}Ga_{0.5}N$ absorber. Moreover, U_{sat} was also found to be strongly dependent on the absorber layer thickness, and simulation yields a saturation voltage of about 35 V for a 500 nm thick $Al_{0.5}Ga_{0.5}N$ absorber, as observed for devices located in the center of the wafer. So in this region, the devices behave as expected. Since the absorber thickness differs only slightly (< 10 nm) over that of the wafer, the observed U_{sat} drop near the edge of the wafer cannot be explained within the model described above.

However, while thickness is relatively homogeneous, inhomogeneously distributed morphological features could be observed by optical microscopy in Nomarski contrast with densities ranging from around $9 \times 10^2 \, cm^{-2}$ in the center to $1 \times 10^4 \, cm^{-2}$ at the edge of the wafer [Figs. 3(a) and 3(b)]. AFM topograms reveal that these hillocks are hexagonal prisms with a diameter of 1–2 μm and a height of about 100 nm having a dip or hole on the top surface [Fig. 3(c)]. Cross-sectional SEM analysis [Fig. 3(d)] shows that the prism has its origin at the $Al_{0.5}Ga_{0.5}N/AlN$ interface, and is associated with the formation of a void. Apparently, a V-pit has formed at this interface causing the formation of inclined Ga-rich regions in the periphery of the void during the $Al_{0.5}Ga_{0.5}N$ growth, which show up as brighter areas in the SEM image. Ga-enrichment is commonly explained by a preferred incorporation of the more mobile Ga atoms at surface steps.[11–13] The surface step in this case is the edge of the V-pit. The higher Ga supply results in a higher growth rate, and thus, the inverted hexagonal prism forms.[14] The void at the $Al_{0.5}Ga_{0.5}N/AlN$ interface is the origin of an open channel most probably bounded by m-plane facets that are visible on the surface. Such "nanopipes" are open-core
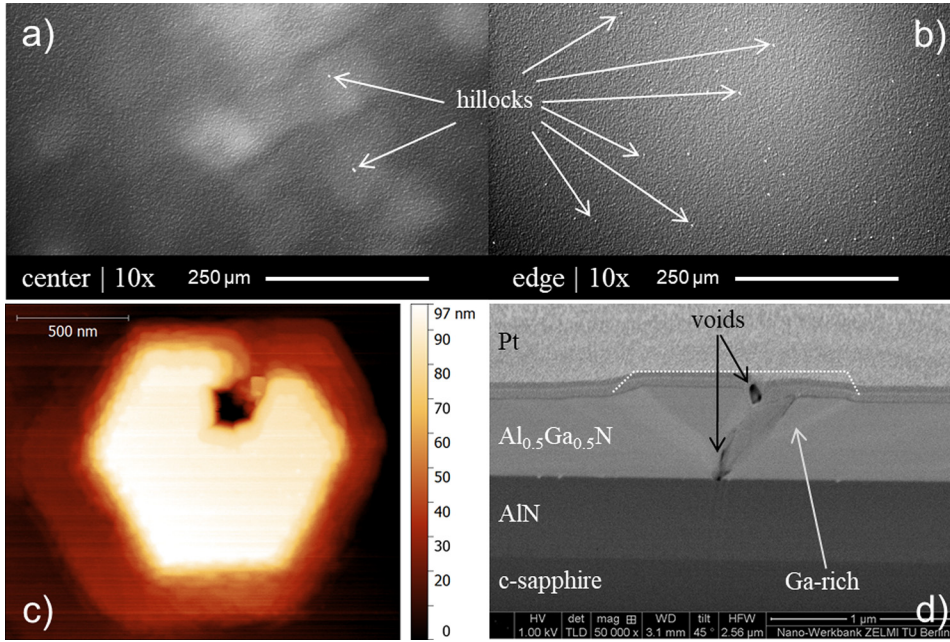
FIG. 3. Images of the $Al_{0.5}Ga_{0.5}N$ surface by optical microscopy ($10\times$ magnification) with Nomarski contrast (a) in the center and (b) at the edge of the 2-in. wafer. Density of hillocks (bright dots): $9 \times 10^2\,cm^{-2}$ (center) and $1 \times 10^4\,cm^{-2}$ (edge). (c) AFM topogram of a typical hillock with a hole in the top facet. (d) SEM image of the FIB cross section through the defect shown in (c).

threading dislocations often observed in III-nitrides.[15,16] They have been identified as electrically active leakage paths.[17,18]

These open-core threading dislocations can be considered as electrically active paths in the model of carrier collection of the MSM PDs as explained in the following (Fig. 4). As described before, an accumulation of photoexcited holes takes place in the polarization-induced SCR_I at the $Al_{0.5}Ga_{0.5}N$/AlN interface. The usual carrier collection mechanism, as described in Ref. 6, relies on the enlargement of the SCR_C below the Schottky electrode with increasing voltage until it sufficiently overlaps with SCR_I enabling an efficient sweep out of the accumulated holes [Fig. 4(a)]. If now an open-core threading dislocation [Fig. 4(b)] electrically connects SCR_C and SCR_I, only a small voltage for the accumulated holes is needed to pass a potential barrier to get into this channel. Therefore, they can be swept out efficiently at a reduced voltage, where SCR_C is not yet in contact with SCR_I, and therefore, the usual collection mechanism does not work. Detectors with no (or only few) such defects show a high value of U_{sat}, which is consistent with the usual carrier

collection mechanism, while detectors with low U_{sat} have around 20 [densities in Figs. 3(a) and 3(b)] of such open-core threading dislocations working as electrically active paths. However, the more efficient collection of carriers still requires that carriers are generated by illumination. So, the conductive channel connecting SCR_C beneath the electrode and SCR_I at the $Al_{0.5}Ga_{0.5}N$/AlN interface does not result in increased dark current. Additionally, it should be noted that the open-core threading dislocations do not have a significant effect on lowering of the Schottky barrier, since for MSM PDs with high density of such dislocations, the dark current is not significantly higher (Fig. 1).

To further promote this extended model of two different carrier collection mechanisms, additional experimental data of MSM PDs with different absorber layer thicknesses of 300 nm, 500 nm, and 1400 nm have been compared (Fig. 5). For all AlGaN thicknesses, MSM PDs with no (or only few) open-core threading dislocations show the usual carrier collection mechanism with U_{sat} being strongly dependent on the absorber layer thickness. MSM PDs that show carrier collection via the shortcut along the nanopipes have the same low value for U_{sat} for all three different absorber layer thicknesses. Since the nanopipes form a highly conductive channel not causing a significant voltage drop, carrier collection is governed by the barriers at the Schottky contact and between the sidewalls of the nanopipes and SCR_I.

IV. SUMMARY AND CONCLUSION

In this study, open-core threading dislocations and their influence on the performance of AlGaN/AlN MSM PDs were analyzed. By extending the recent model of carrier collection in such devices, it could be concluded, that these dislocations act as highly conductive paths bypassing the AlGaN absorber layer. The MSM PDs are improved by a critical density of open-core threading dislocations showing high EQE at a reduced bias voltage while dark current remains low.
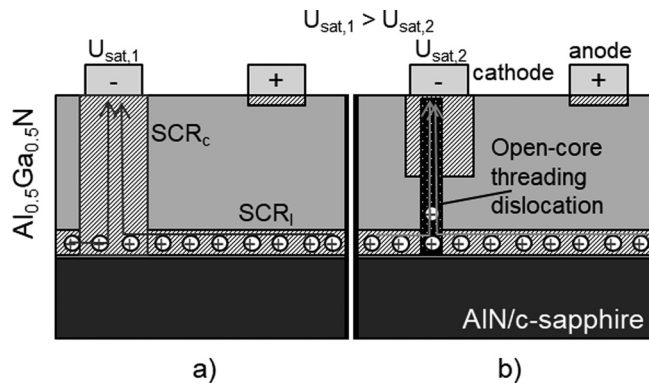

FIG. 4. Sketch of an MSM PD illustrating the two different carrier collection mechanisms. (a) The SCR_C is vertically fully extended and in contact with SCR_I at the interface. (b) Open-core threading dislocation connecting SCR_C and SCR_I at a reduced voltage.
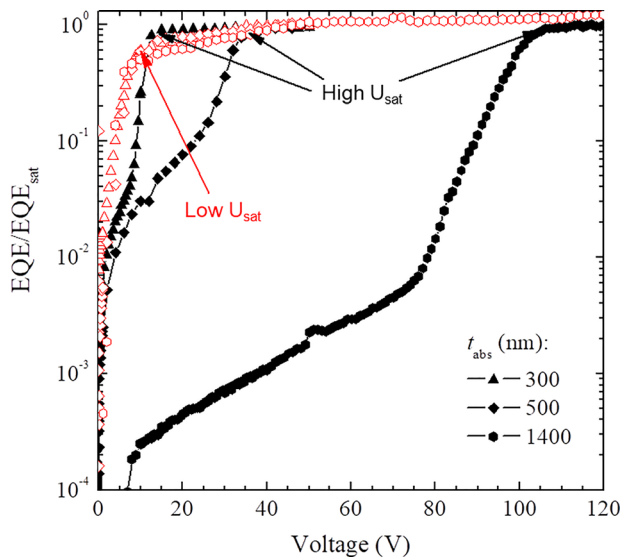
FIG. 5. EQE vs. bias characteristics of MSM PDs with absorber layer thicknesses between 300 nm–1400 nm illuminated from the bottom side at a wavelength of 250 nm. MSM PDs with the black curves (filled symbols) show the usual carrier collection mechanism and MSM PDs with the red curves (empty symbols) show the carrier collection mechanism induced by open-core threading dislocations.

With respect to the usual observation of open-core threading dislocations being responsible for high leakage currents in devices like LEDs, it is interesting to note that this effect can also be beneficial for the bias-dependent operation of MSM photodetectors. However, to design a device based on open-core threading dislocations working as conductive channels, further work has to be done to control and manipulate the densities of those defects.

ACKNOWLEDGMENTS

[1]J. Long, S. Varadaraajan, J. Matthews, and J. Schetzina, Opto-Electron. Rev. **10**, 251 (2002).
[2]M. Razeghi, IEEE Proc. **90**, 1006 (2002).
[3]L. Sang, M. Liao, and M. Sumiya, Sensors **13**, 10482 (2013).
[4]I. Vurgaftman, J. R. Meyer, and L. R. Ram-Mohan, J. Appl. Phys. **89**(11), 5815 (2001).
[5]J. Guohua, Z. Yizhou, D. Yuming, L. Yuanfu, and L. Jiancheng, IEEE (RCAR) **321**, 321–325 (2016).
[6]M. Brendel, M. Helbling, A. Knigge, F. Brunner, and M. Weyers, J. Appl. Phys. **118**, 244504 (2015).
[7]E. Cicek, R. Mc Clintock, Z. Vashaei, Y. Zhang, S. Gautier, C. Cho, and M. Razeghi, Appl. Phys. Lett. **102**, 051102 (2013).
[8]J. Ohsawa, T. Kozawa, H. Miura, O. Fujishima, and H. Itoh, Jpn. J. Appl. Phys., Part 1 **44**, 8441 (2005).
[9]B. Yang, D. J. H. Lambert, T. Li, C. Collins, M. Wong, U. Chowdhury, R. Dupuis, and J. Campbell, Electron. Lett. **36**, 1866 (2000).
[10]M. Brendel, M. Helbling, A. Knauer, S. Einfeldt, A. Knigge, and M. Weyers, Phys. Status Solidi A **212**, 1021 (2015).
[11]A. Mogilatenko, V. Küller, A. Knauer, J. Jeschke, U. Zeimer, M. Weyers, and G. Tränkle, J. Cryst. Growth **402**, 222 (2014).
[12]U. Zeimer, V. Kueller, A. Knauer, A. Mogilatenko, M. Weyers, and M. Kneissl, J. Cryst. Growth **377**, 32 (2013).
[13]A. Knauer, U. Zeimer, V. Kueller, and M. Weyers, Phys. Status Solidi C **11**, 377 (2014).
[14]A. Mogilatenko, J. Enslin, A. Knauer, F. Mehnke, K. Bellmann, T. Wernicke, M. Weyers, and M. Kneissl, Semicond. Sci. Technol. **30**, 114010 (2015).
[15]S. K. Hong, T. Yao, B. J. Kim, S. Y. Yoon, and T. I. Kim, Appl. Phys. Lett. **77**, 82 (2000).
[16]W. Qian, G. S. Rohrer, M. Skowronski, K. Doverspike, L. B. Rowland, and D. K. Gaskill, Appl. Phys. Lett. **67**, 2284 (1995).
[17]M. Moseley, A. Allerman, M. Crawford, J. J. Wierer, M. Smith, and L. Biedermann, J. Appl. Phys. **116**, 053104 (2014).
[18]M. Moseley, A. Allerman, M. Crawford, J. J. Wierer, M. Smith, and A. M. Armstrong, J. Appl. Phys. **117**, 095301 (2015).